Time of flight secondary ion mass spectrometry and high-resolution transmission electron microscopy/energy dispersive spectroscopy: A preliminary study of the distribution of Cu^{2+} and Cu^{2+}/Pb^{2+} on a Bt horizon surfaces

B. Cerqueira [a], F.A. Vega [a], C. Serra [b], L.F.O. Silva [c], M.L. Andrade [a,*]

[a] Department of Plant Biology and Soil Science, Faculty of Biology, University of Vigo, Lagoas, Marcosende, 36310 Vigo, Pontevedra, Spain
[b] CACTI, University of Vigo, Campus Lagoas-Marcosende, 36310 Vigo, Spain
[c] Environmental Science and Nanotechnology Department, Catarinense Institute of Environmental Research and Human Development – IPADHC, Capivari de Baixo, Santa Catarina, Brazil

ARTICLE INFO

ABSTRACT

Relatively new techniques can help in determining the occurrence of mineral species and the distribution of contaminants on soil surfaces such as natural minerals and organic matter.

The Bt horizon from an Endoleptic Luvisol was chosen because of its well-known sorption capability. The samples were contaminated with Cu^{2+} and/or Pb^{2+} and both sorption and desorption experiments were performed. The preferential distribution of the contaminant species (^{63}Cu and ^{208}Pb) to the main soil components and their associations were studied together with the effectiveness of the surface sorption and desorption processes. The results obtained were compared with non-contaminated samples as well as with previous results obtained by different analytical techniques and advanced statistical analysis. Pb^{2+} competes favorably for the sorption sites in this soil, mainly in oxides and the clay fraction. Cu^{2+} and Pb^{2+} were mainly associated with hematite, gibbsite, vermiculite and chlorite.

This study will serve as a basis for further scientific research on the soil retention of heavy metals. New techniques such as spectroscopic imaging and transmission electron microscopy make it possible to check which soil components retain heavy metals, thereby contributing to propose effective measures for the remediation of contaminated soil.

© 2011 Elsevier B.V. All rights reserved.

1. Introduction

The bioavailability of heavy metals and other soil pollutants and the risk that they reach surface or underground waters mainly depend on the sorption and desorption capacity of soil components. The term "sorption" is used to encompass adsorption, precipitation on soil particle surfaces, and fixation and "desorption" for the release of sorbed species to the surrounding environment [1–3]. The sorption and desorption of cations predominantly involve negatively charged soil surfaces such as organic matter, clays and metallic oxides or hydroxides [3]. The distribution of metals among the soil components depends on the intrinsic properties of the metal species involved, the properties of the soil, and the amounts of metal added [4,5].

The immobilization of copper and lead in soils occur as a result of several processes, such as adsorption, chemisorption, ion exchange, or surface precipitation. Soil organic matter is an important sorbent for lead and, to a lesser extent, for copper [6]. Both ions are also bound by specific adsorption and precipitation in calcareous soils on calcite surfaces [7,8].

Soil iron minerals and hydrous iron and manganese oxide surfaces also play an important role in copper and lead sorption [9–11]. Clays such as smectite and vermiculite are well known as important sorbents of copper and lead.

A large number of articles refer to heavy metal sorption on soils and soil components, and the experiments involved included techniques such as chemical extractions, batch and soil column sorption experiments [11–14]. Few of the papers that have been published have focused on advanced electron microscopy techniques to study the association of metals to different soil particles [15].

In previous publications [3,16–19] several soils were characterized and sorption and desorption isotherms were determined in order to evaluate both monometal and competitive sorption capacities. The influence of soil properties was established by means of advanced statistical analyses [19]. The analyses revealed that the soils with the highest pH, effective cation exchange capacities

---

(CECe) and Mn and Fe oxide contents, as well as those with the greatest mineralogical variety in the clay fraction, have the highest capacity for the individual and competitive sorption of Cu^{2+} and Pb^{2+}. The sorption of Cu^{2+} and Pb^{2+} appears to take place almost exclusively through cation exchange [19].

Since the surface chemistry exerts a major influence on chemical species and their eventual fate, the characterization of different chemicals on mineral and organic surfaces of natural samples is an important topic. The soil surface chemistry can vary considerably on a microscopic scale, and this heterogeneity or variability can lead to misinterpretation, introducing confusion in the characterization process.

Relatively new spectroscopic imaging techniques can help in determining the distribution of contaminants on soil surfaces such as natural minerals and organic matter. The secondary ion mass spectrometry (SIMS) technique was developed about 60 years ago [20]. Later, the idea was to provide spatially resolved information with SIMS and that it should be possible to build an ion-optical collection system, analogous to a lens used in the light microscope, preserving the spatial relationship of the desorbed ions, as reviewed by Benninghoven et al. [21] and Benninghoven [22]. The principle of TOF (time of flight) coupled with SIMS is based on the fact that ions with different masses travel at different speeds. Basically, desorbed secondary ions from the target surface are accelerated by an electrostatic field and they travel to the detector.

The TOF-SIMS technique makes it possible to determine the presence of a wide range of air, soil and water pollutants. Owing to an application of TOF-SIMS, processes involving adsorption and the migration of toxic substances in different environments can be observed, as well as pollution mechanisms. Generally, TOF-SIMS experiments concentrate on measuring the surface composition of analyzed materials and the distribution of particular components on the surface of the investigated samples [23]. This technique is one of the most surface-sensitive analytical techniques and has several advantages over alternative imaging methods, such as its sensitivity to all elements, detection of their isotopes, fast data acquisition due to a parallel detection system, very low sampling depth (1–2 nm), sensitivity in the part per million (ppm) to part per billion (ppb) in most of the species range, and the ability to successfully analyze insulators.

Also, the occurrence of mineral species can be investigated by means of X-ray diffraction (XRD), environmental field emission scanning electron microscopy (FE-SEM) with energy-dispersive X-ray spectrometer (EDS) capabilities for chemical analyses of individual particles, and high-resolution transmission electron microscope (HR-TEM) with selected area electron diffraction (SAED) and/or microbeam diffraction (MBD), and scanning transmission electron microscopy (STEM).

The aim of this study is to detect Cu^{2+} and Pb^{2+} in soil surfaces applying TOF-SIMS and HR-TEM/EDS techniques, comparing non-contaminated and contaminated samples (treated with one or both ions, and after sorption and desorption experiments). The results obtained are compared with previous results obtained by different analytical techniques [3,18]. The preferential distribution of contaminant species ([63]Cu and [208]Pb) at the main soil components and their associations were studied, together with the effectiveness of the surface sorption and desorption processes.

2. Material and methods

2.1. Soil samples

The Bt horizon from an Endoleptic Luvisol (EL) [24] was chosen to perform this work because of its well-known high sorption and retention capacities and soil properties [3]. Statistical techniques

Table 1
Soil characteristics.

pH		6.40
Organic carbon (g kg^{-1})		5.82
Effective cation exchange capacity and exchangeable cation content (cmol$_{(+)}$ kg^{-1})	CECe	62.16
	Na	0.69
	K	0.22
	Ca	2.70
	Mg	58.35
	Al	0.20
Oxide content (g kg^{-1})	Al$_2$O$_3$	3.25
	Fe$_2$O$_3$	30.07
	MnO	0.36
Particle size distribution (%)	Sand	21.30
	Silt	12.60
	Clay	66.10
Clay content (% of clay fraction)	Vermiculite	60
	Gibbsite	12
	Chlorite	20
	Kaolinite	8
Specific surface area (m^2 g^{-1})		78
Major elements (total content, %)	Na$_2$O	0.7
	MgO	16.6
	Al$_2$O$_3$	7.1
	SiO$_2$	37.3
	P$_2$O$_5$	ul
	K$_2$O	0.3
	CaO	3.9
	TiO$_2$	0.3
	Fe$_2$O$_3$	18.7
Trace elements (total content, mg kg^{-1})	V	87
	Cr	331
	Mn	1710
	Co	125
	As	ul
	Cd	1
	Ni	233
	Cu	47
	Zn	29
	Rb	14
	Sr	84
	Ba	96
	Pb	24
	Cl	ul

ul, undetectable level.

such as regression and correlation analysis were used to assess the influence of their components and properties on the sorption and desorption of monometal (Cu^{2+}) and competitive (Cu^{2+} and Pb^{2+}) species [18]. Sorption and retention capacities mainly depend on pH, CECe, and organic matter, Mn and Fe oxides and clay contents. Vermiculite and chlorite are the clay minerals that most influence these fixation capacities. Table 1 shows the main soil horizon properties of Bt.EL.

2.2. Sample treatment

Sorption solutions of a single-metal solution (3 mM Cu(NO$_3$)$_2$) and a bi-metal solution (3 mM Cu(NO$_3$)$_2$ and 3 mM Pb(NO$_3$)$_2$) with 0.01 M NaNO$_3$ as background electrolyte were prepared. Next, 6 g of soil and 100 ml of each sorption solution were placed in polyethylene jars and shaken in a rotary shaker for 24 h at 25 °C, then centrifuged at 5000 rpm and filtered through Whatman 42 paper. The resulting filtrate was analyzed by inductively coupled plasma optical emission spectrometry (ICP-OES) in a Perkin–Elmer Optima 4300 DV device. The amount of each metal that had been sorbed was calculated from the difference between its concentrations in solution before the addition of soil and after equilibration (sorbed metal = concentration of the added solution − concentration in solution at equilibrium).
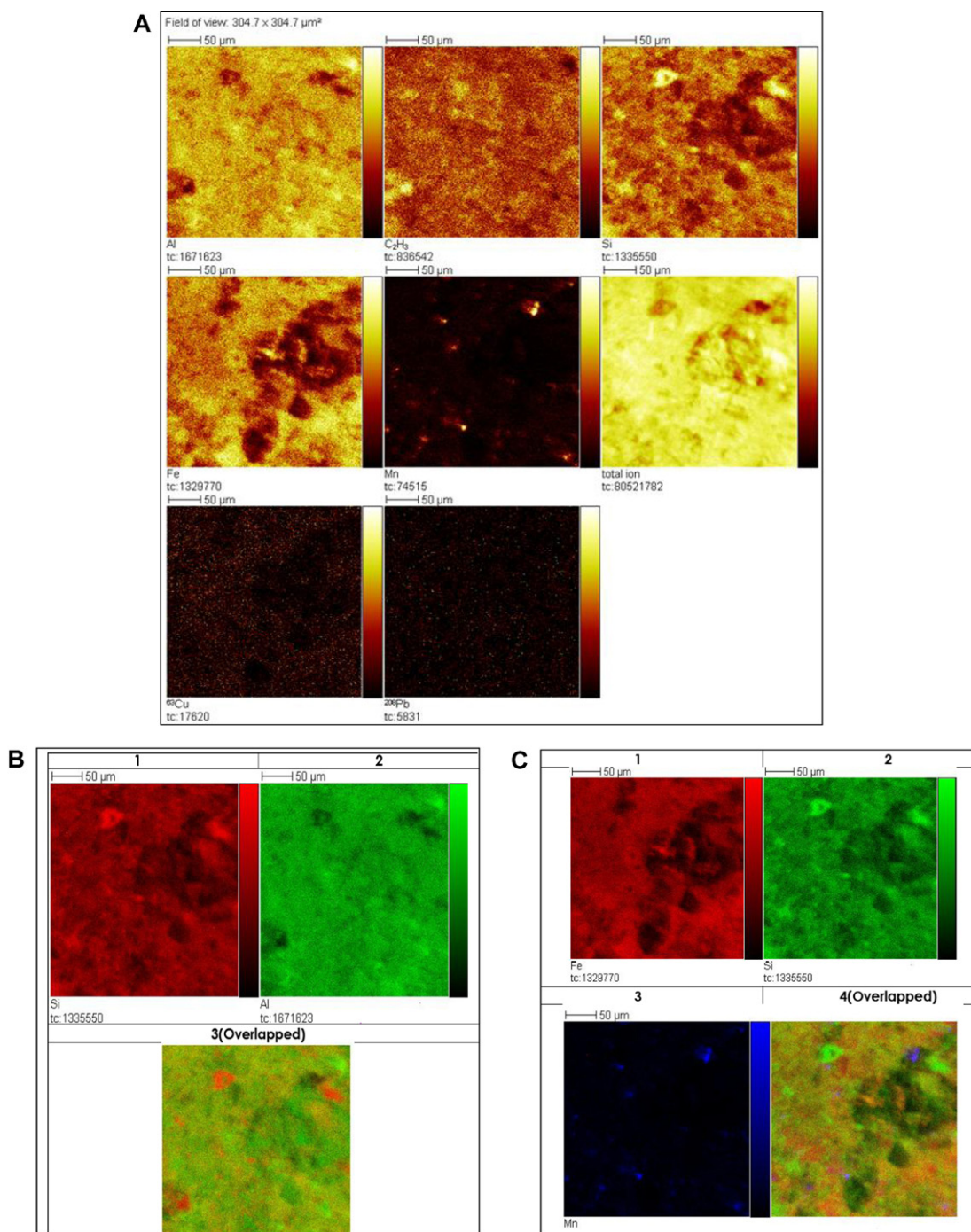
Fig. 1. Untreated soil (CS sample). (A) TOF-SIMS image of Al, C_2H_3, Si, Fe and Mn, and overlapping all the signals with ^{63}Cu and ^{208}Pb, there is no signal of the last two. (B) Image of overlapping Si and Al showing the concordance between both signals. (C) Image of overlapping Fe, Si and Mn showing the concordance between all signals.

The desorption experiments were performed using the pellets obtained after the sorption stage. They were dried at $45\,^{\circ}C$ and weighed to check if any of the soil sample had been lost during the sorption filtration stage. 100 ml of 0.01 M $NaNO_3$ solution were added to each sample and then shaken for 24 h. The following procedure is the same as in the sorption experiments. The amount of metal retained after the sorption experiments was calculated by subtracting the concentration of the metal in solution following desorption from the previously sorbed amount.

2.3. Analyzing untreated soil samples and samples after sorption and desorption of Cu^{2+} and $Cu^{2+} + Pb^{2+}$ by TOF-SIMS

Time of flight secondary ion mass spectrometry (TOF-SIMS IV instrument from Ion-TOF GmbH of Münster, Germany) was used to investigate the elemental and molecular structure of the samples and to obtain a clearer understanding of the chemical composition [25], location and relative abundance of the species present at the surface of the soil sample.
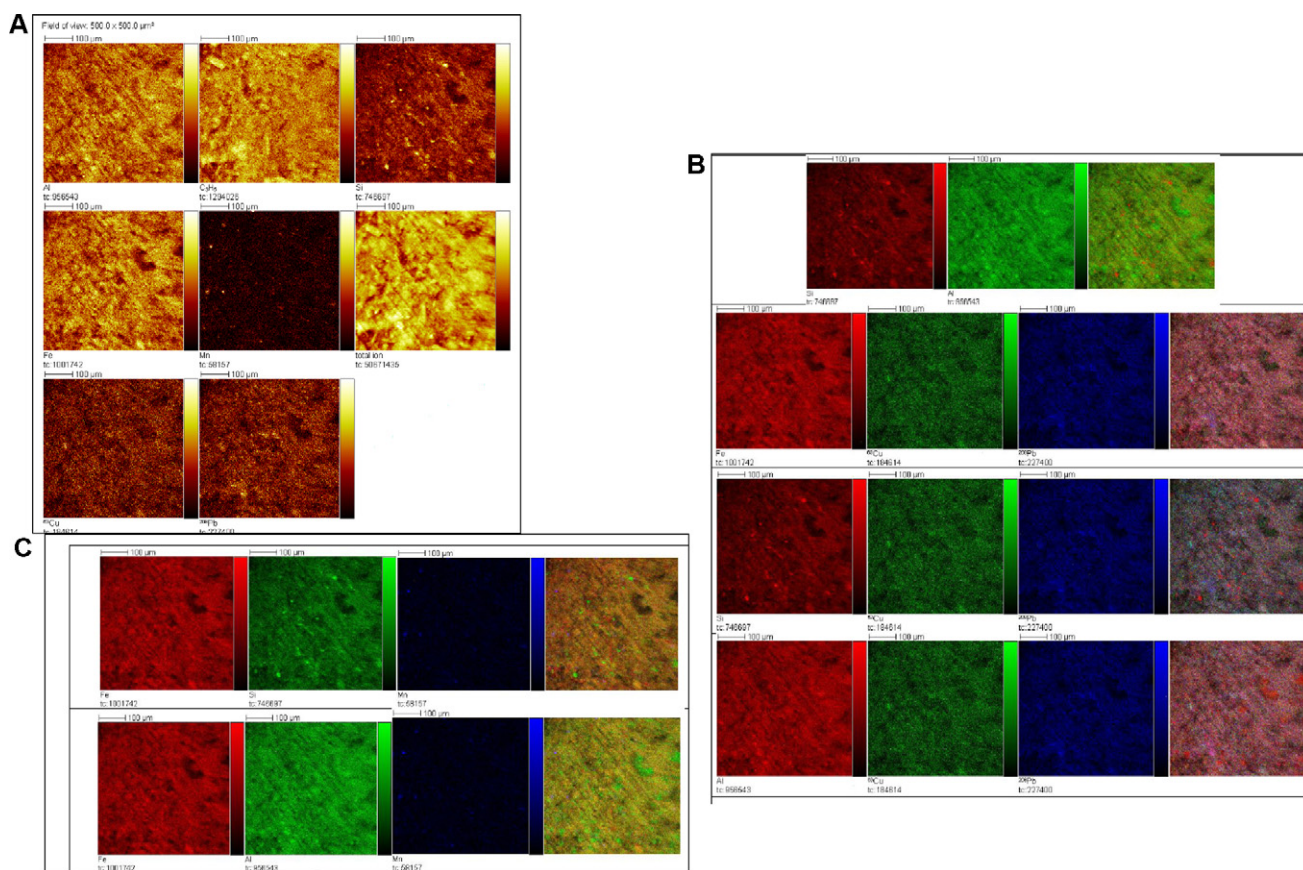
Fig. 2. Soil treated with Cu^{2+} and Pb^{2+} after sorption process (CS sample). TOF-SIMS images of overlapping all the signals with ^{63}Cu and ^{208}Pb showing the concordance.

The TOF analyzer separates the ions according to the time they take to travel through the length of the field-free flight-tube. This time interval is related to the mass and charge of the accelerated particles. The energy and angular dispersion of the secondary ions can be compensated using focusing elements such as a reflectron. The lighter secondary ions arrive before the heavier ones whereby a mass spectrum can be recorded.

TOF-SIMS works by focusing and scanning a narrow pulsed ion beam on the surface. This process leads to the emission of charged secondary ions in a sputtering process from the outermost surface of the sample. Further analysis of the secondary ions provides information on the molecular and elemental species and their isotopes present on the surface. The secondary ions collected and represented in the mass spectra can be attributed to complete molecules, large fragments of molecules that have only lost functional groups.

TOF-SIMS analysis was performed with Bt.EL untreated soil samples and those samples obtained after sorption and desorption experiments. During the TOF-SIMS experiment the corresponding sample was bombarded with a pulsed bismuth ion beam. The secondary ions generated were extracted with a 10 kV voltage and their time of flight from the sample to the detector was measured in a reflection mass spectrometer.

The analysis conditions were: 25 keV pulsed Bi^{3+} beam at 45° incidence, rastered over 304 µm × 304 µm; at a square-pixel density of 256 × 256, and 50 accumulative scans in each analyzed area. The operating pressure in the main chamber was 5×10^{-10} mbar. An Electron Flood Gun (low energy electrons) was used to compensate the surface charge build-up process during the experiment. Positive secondary ion mass spectra were acquired over a mass range from $m/z = 0$ to $m/z = 1000$. Negative ion TOF-SIMS spectra were not considered in this study. The mass resolution ($m/\Delta m$) of the secondary ion peaks in the positive spectra was typically between 3600 and 6000. Before further analysis the positive spectra were calibrated using CH$_3^+$, C$_2$H$_3^+$, C$_3$H$_5^+$, and C$_7$H$_7^+$ ions.

To obtain two-dimensional imaging (chemical surface maps), polyatomic bismuth projectiles (Bi^{3+}) were focused onto the surface in a rastered mode. The detected intensities for secondary ion signals were color-coded according to a color scale. The chemical maps produced by TOF-SIMS represent the ions that reached the detector rather than the ions that were present on the surface. Because each solid has its own ability to release ions, the intensities cannot be used to derive absolute surface concentrations. However, the chemical maps are very useful for indicating the relative surface abundance and how it changes as a function of time or sample treatment.

The studied ions (Table 2) are Al, Fe, Mn, Si and C$_3$H$_5^+$ (as representative elements of main soil components) and ^{63}Cu and ^{208}Pb (as soil pollutants).

Table 2
Ions represented in the maps.

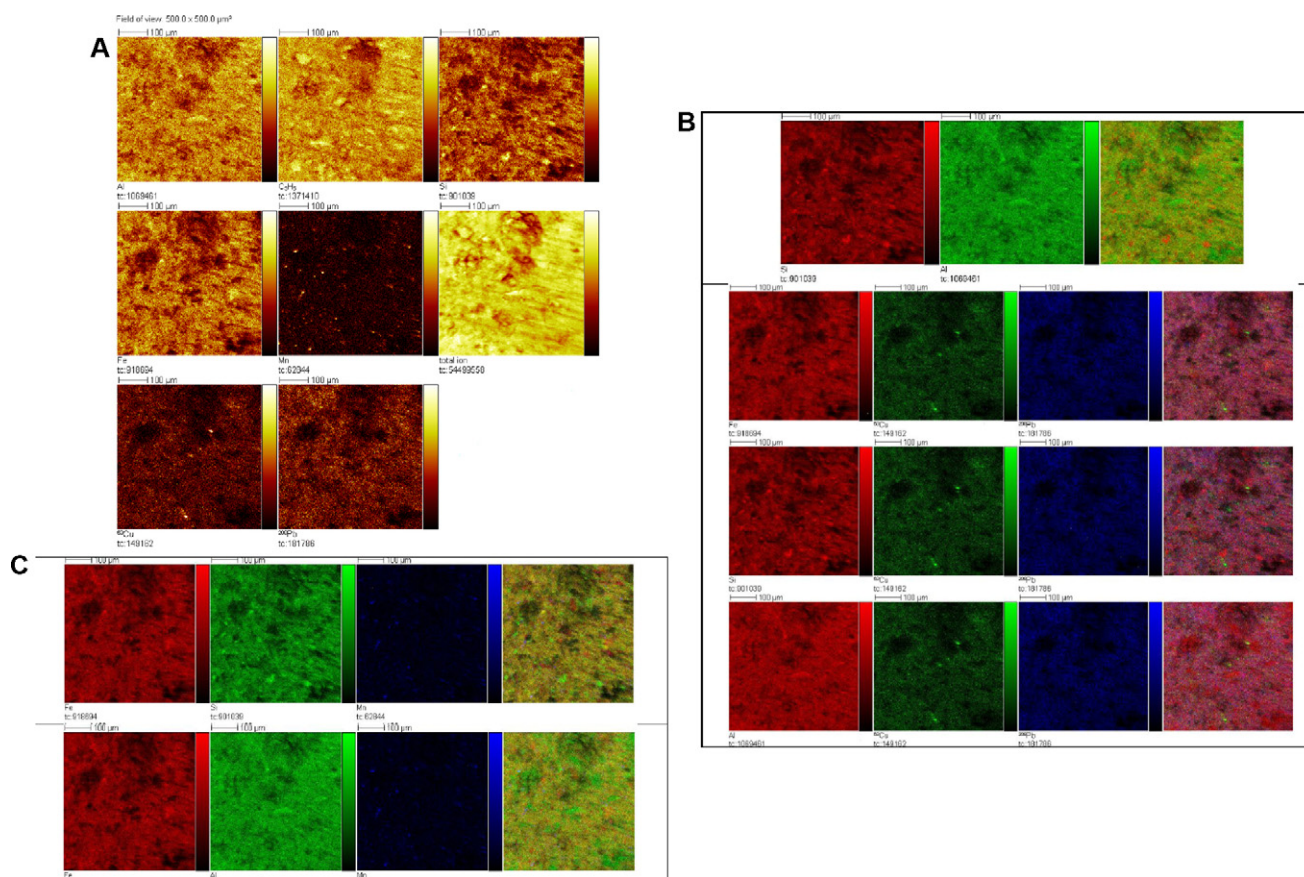| Ion	Centre mass	Resolution
Al	26.9798	4204
Si	27.9723	4232
C$_3$H$_5^+$	41.0389	3633
Mn	54.9364	3687
Fe	55.9299	6024
^{63}Cu	62.9277	4168
^{208}Pb	207.9558	5527

Fig. 3. Soil treated with Cu^{2+} and Pb^{2+} after desorption process (CD sample). TOF-SIMS images of overlapping all the signals with [63]Cu and [208]Pb showing the concordance.

2.4. Soil analysis by advanced electronic beam

The occurrence of mineral and nanoparticles species was investigated by means of XRD, FE-SEM with EDS and HR-TEM with SAED or MBD, and STEM.

Analysis of XRD was used to determine crystalline phases in the studied samples (Siemens model D5005 X-ray diffractometer). The samples were ground by hand in a ceramic mortar and pestle, dry mounted in aluminum holders, and scanned at 8–6° 2θ with Cu K-α radiation [26,27].

The morphology, structural distribution, and particle chemical composition of samples containing ultrafine particles and minerals (crystalline and/or amorphous) were examined using a Zeiss Model ULTRA plus FE-SEM (with charge compensation for all applications on conductive as well as non-conductive samples) and a 200 kV Zeiss-LIBRA® 200FE HR-TEM (information limit < 0.08 nm at 200 kV) equipped with high efficient field emission cathode and energy omega-filter for high-accuracy measurements of structure and atomic composition of nano-sized minerals at ultimate resolution. The precession interface module with HR-TEM makes it possible to work at a maximum precession angle of up to 5°, and saves different alignments for different precession electron diffraction (PED) angles in memory; the module can correct on-line spot size aberration effects caused by high precession angles.

Structure determination of nanominerals with PED has been proved to be highly successful in TEM for a variety of nanocrystals ranging from oxides, sulphates, and other minerals [28–31]. The FE-SEM was equipped with an EDS and the mineral identifications were made on the basis of morphology and grain composition using both secondary electron and back-scattered electron modes [32,33]. Geometrical aberrations were measured by HR-TEM and

controlled to provide less than a $\pi/4$ phase shift of the incoming electron wave over the probe-defining aperture of 14.5 mrad [34,35]. EDS spectra were recorded in FE-SEM images mode and then quantified using ES Vision software that uses the thin-foil method to convert X-ray counts of each element into atomic or weight percentages [36]. Electron diffraction patterns of the crystalline phases were recorded in SAED or MBD mode, and the d spacings were compared to the International Center for Diffraction Data [37] inorganic compound powder diffraction file (PDF) database to identify the crystalline phases.

The soil samples were analyzed after the desorption process due to the importance of knowing the distribution between soil particles, especially in the case of high sorption hysteresis such as that found in the soil studied for both metals [17,18].

2.5. Statistical analyses

All analyses were performed in triplicate and all statistical calculations were performed using SPSS for Windows, version 14.0.

3. Results and discussion

The sorbed and retained concentrations of Cu^{2+} and Pb^{2+} in each treatment are shown in Table 3. This soil has a greater affinity for Pb^{2+} than for Cu^{2+} because Pb^{2+} competes favorably for sorption sites on soil components [3]. This is because the amount of Pb^{2+} (both sorbed and retained after sorption) is higher than the amount of Cu^{2+} when they are added together. Iron and manganese oxides and clay contents (particularly vermiculite and chlorite) are well correlated with the amounts of sorbed and retained ions after using statistical analysis [19]. Cu^{2+} and Pb^{2+} sorption was almost irre-
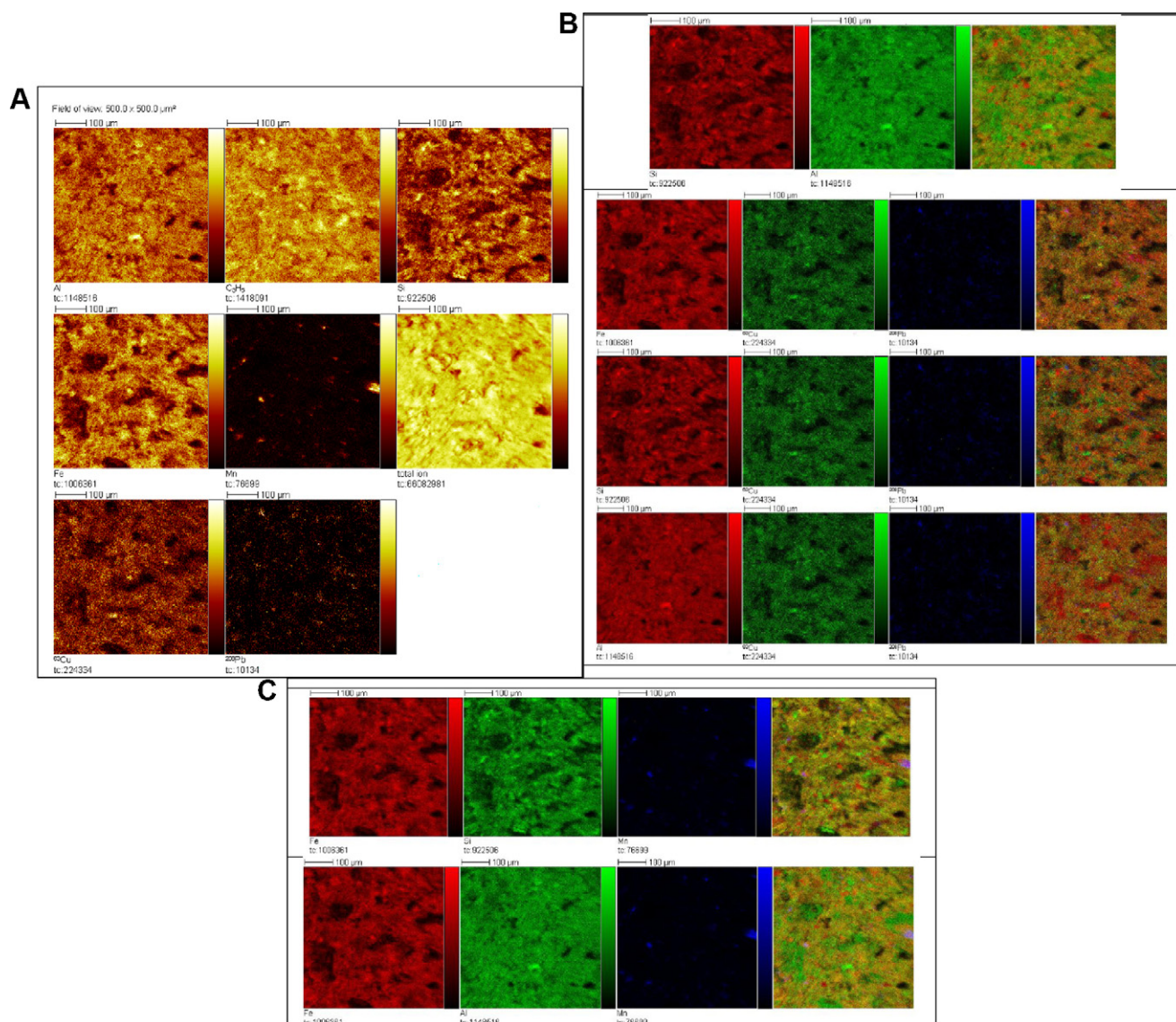
Fig. 4. Soil treated with Cu^{2+} after sorption process (MS sample). TOF-SIMS images of overlapping all the signals with ^{63}Cu showing the concordance.

versible (Table 3), which indicates the high fixation capacity of this soil horizon.

3.1. TOF-SIMS experiments

The TOF-SIMS technique makes it possible to determine the spatial ion distribution of contaminant species (^{63}Cu and ^{208}Pb) and to verify the association of Cu^{2+} and Pb^{2+} to soil components.

The results from soil samples, before and after sorption experiments (uncontaminated soil, and soil contaminated with one or both cations after sorption and desorption processes) are discussed below.

Figs. 1–5 show the map distribution of the surface ions from TOF-SIMS. These images show the lateral distribution of specific chemical species on the sample surface, within a randomly chosen area ($304\,\mu m \times 304\,\mu m$) on the sample. On the left of each image is

Table 3
Sample name and Cu^{2+} and Pb^{2+} soil content.

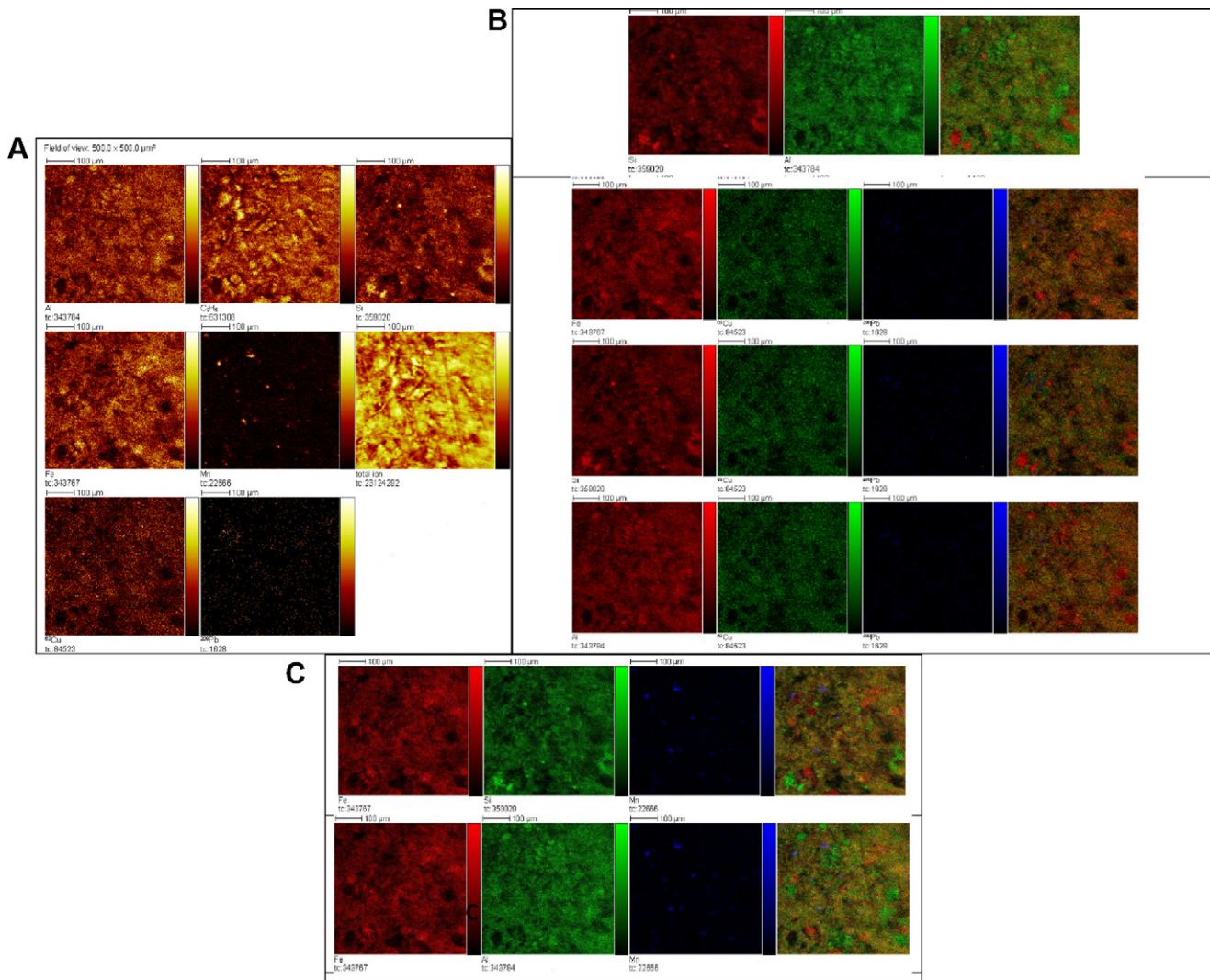| Studied soil	Treatment, samples, nomenclature and Cu^{2+} and Pb^{2+} sorbed and retained	
Bt horizon from Endoleptic Luvisol developed over serpentinized amphibolite	Untreated sample (US)	
	Monometallic (Cu^{2+}) sorption (MS)	
	Sorbed Cu^{2+}: 47.55 $\mu mol\,g^{-1}$	
	Monometallic (Cu^{2+}) desorption (MD)	
	Retained Cu^{2+}: 46.77 $\mu mol\,g^{-1}$	
	Competitive ($Cu^{2+} + Pb^{2+}$) sorption (CS)	
	Sorbed Cu^{2+}: 42.21 $\mu mol\,g^{-1}$	Sorbed Pb^{2+}: 43.33 $\mu mol\,g^{-1}$
	Competitive ($Cu^{2+} + Pb^{2+}$) desorption (CD)	
	Retained Cu^{2+}: 40.04 $\mu mol\,g^{-1}$)	Retained Pb^{2+}: 42.32 $\mu mol\,g^{-1}$

Fig. 5. Soil treated with Cu^{2+} after desorption process (MD sample). TOF-SIMS images of overlapping all the signals with ^{63}Cu showing the concordance.

the intensity bar (the signal intensity of each ion). The dark color means no signal; in these points the detection limit for this ion was reached. The lightest color represents the maximum signal intensity and shows the points of maximum ion abundance. The corresponding ion is indicated in the bottom left-hand side of each image. Below in the graph is the TC (number of total counts of each ion).

By overlaying the three images with red, green and blue colors, it is possible to identify matching distributions of ions on the sample surface. In the overlaid image, areas can appear with a single color (red, green or blue) but also areas with different colors. These areas with colors other than red, green or blue are those where more than one ion is located. These new colors are the product of mixing the first. Thus, red + green = orange; red + blue = purple and green + blue = yellow. If the three main colors (red, green and blue) occur at the same point, the final result is a white region or point.

Fig. 1 shows the results from untreated soil. There is no signal for Cu^{2+} and Pb^{2+}, but when soils are treated with one or both ions (Figs. 2–5) the signal is clear and more intense before the desorption process (Figs. 2 and 3). The maps also show that ^{63}Cu and ^{208}Pb (when possible) have the same distribution in terms of spatial intensity, and they also show good concordance with the distribution of iron (^{56}Fe) and manganese (^{55}Mn). There is a slightly poorer relation between the spatial intensity distribution of both ^{63}Cu and ^{208}Pb and that of silicon and aluminum ions. The association of Pb^{2+} with $C_3H_5^+$ is not very intense, but is higher than that of Cu^{2+}.

TOF-SIMS illustrates the coincidence of Al-, Fe-, Mn-, Si- and Cu^{2+} and Pb^{2+} bearing areas (Figs. 2–5). This can be explained due to an association of clay and oxides, but does not provide any additional information on the dominance of any single Cu^{2+} or Pb^{2+} association.

On the other hand, the desorption process in both types of treatments leads to a reduction in the extent to which the soil is contaminated. Nevertheless, there are differences in the effectiveness of the desorption process between both types of treatments. For example, in the monometal sorption (MS) sample, the effectiveness of copper desorption is lower than in the competitive sorption (CS) sample, because there is no competition with Pb^{2+} and Cu^{2+} is more strongly retained in MS.

The close relationship found between the metals and soil components that were studied (particularly iron and manganese oxides, clay and organic matter, the latter especially for Pb^{2+}) is in line with previous results [18]. Image analysis by TOF-SIMS is an excellent method for completing and verifying the results of sorption and desorption studies. Fig. 6 shows the spectrum comparison of untreated and treated soil: (I) Pb isotope group: ^{208}Pb (amu: 208), ^{207}Pb (amu: 207), ^{206}Pb (amu: 206), and (II) zone ^{208}Pb (amu: 208). The TOF-SIMS peaks between the region of mass 205.5 amu and
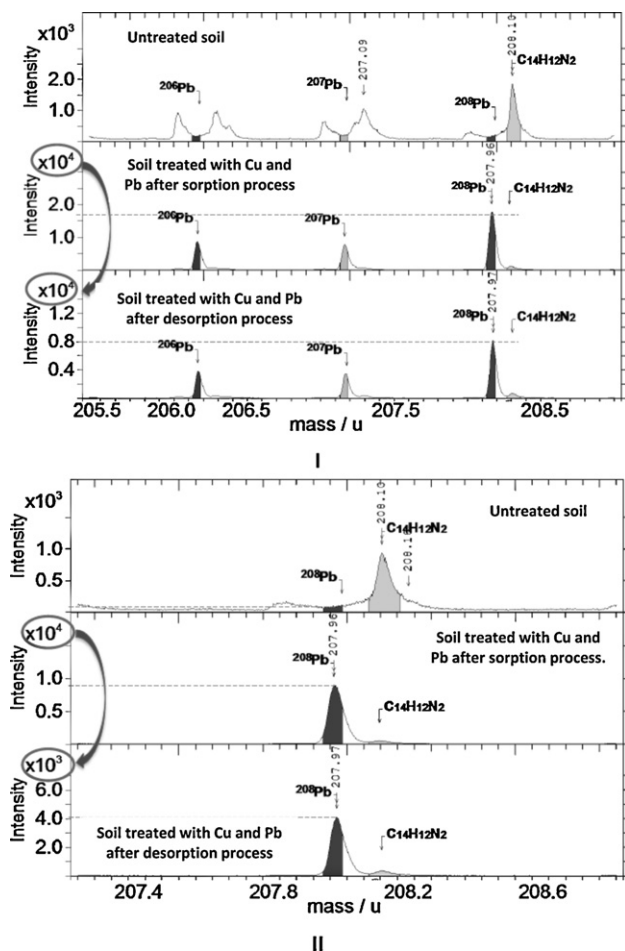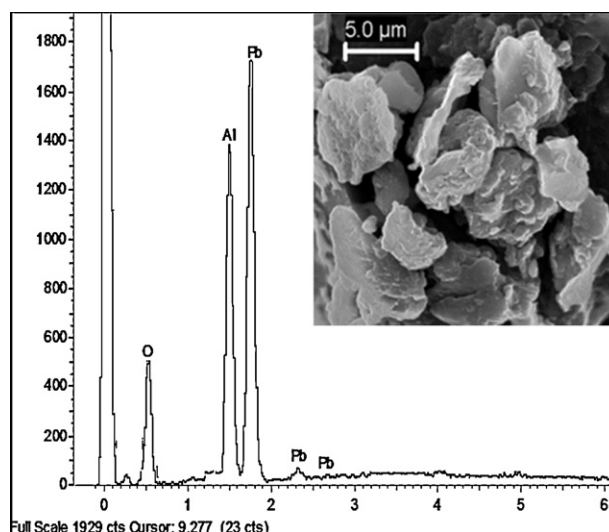
Fig. 8. Soil treated with Pb^{2+}: EDS spectrum of gibbsite containing Pb.

Table 4
Comparison of the calculated ratios from normalized intensity of ions between the total counts of Si and the total counts of Cu^{2+} and Pb^{2+} ($I = ISilicon/IPollutant$).

Sample	Ratio $I ^{28}$Si/$I ^{208}$Pb	Ratio $I ^{28}$Si/$I ^{63}$Cu
US (untreated soil)	229	75.8
MS (copper sorbed soil)	91.03	4.11
MD (copper desorbed soil)	220.5	4.24
CS (copper and lead sorbed soil)	4.05	3.28
CD (copper and lead desorbed soil)	6.04	4.95

208.5 amu are shown in Fig. 6. In this region, we detected ^{208}Pb, ^{207}Pb and ^{206}Pb, but the most abundant and representative type in the Pb^{2+} contaminated samples is ^{208}Pb. Fig. 7 also shows the comparison of spectra of untreated and treated soil for the zone ^{63}Cu (amu: 63).

Although TOF-SIMS is not a quantitative technique, the ratios between the total counts of silicon (Si, amu = 28) (chosen as element representative of the soil) and the total counts of the contaminant elements (Cu^{2+} and Pb^{2+}) were calculated by comparing the spectra. These ratios (Table 4) were taken as a qualitative reference for the effectiveness of the desorption process. The higher the ratio value in desorbed samples (compared to that from non-contaminated samples), the more effective the desorption process.

The ratios (Table 4) are also consistent with the results obtained in previous studies. The advantages of the TOF-SIMS technique in
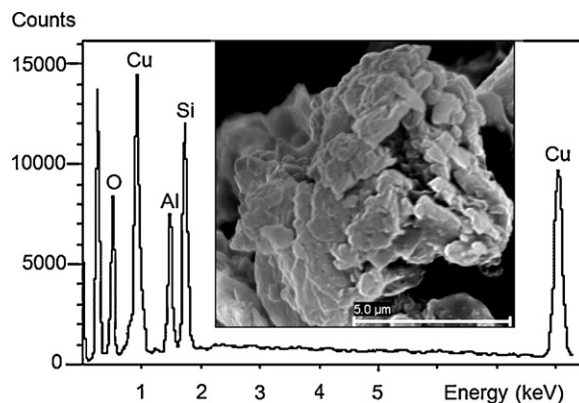

Fig. 6. TOF-SIMS spectra of Pb isotopes of untreated and treated soil (I). Spectra comparison/positive polarity: ^{208}Pb zone (amu: 208) (II).
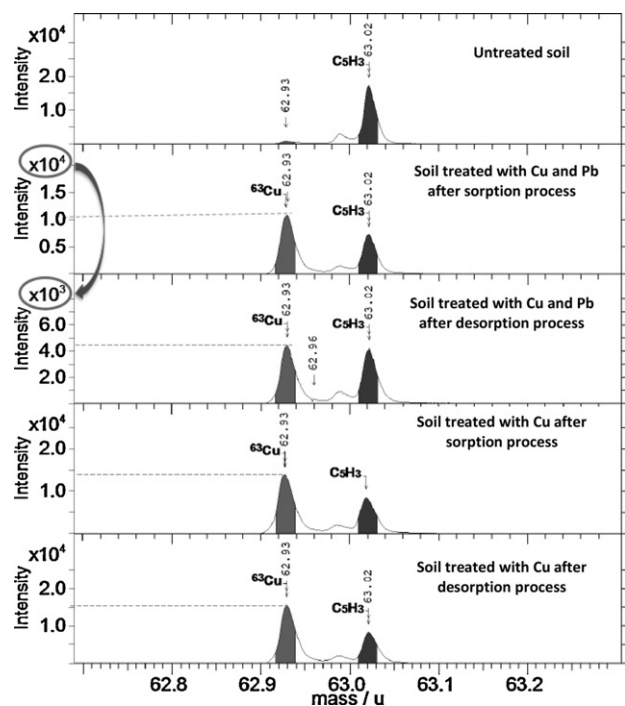
Fig. 7. TOF-SIMS spectra of ^{63}Cu of untreated and treated soil. Spectrum comparison/positive polarity. ^{63}Cu zone (amu: 63).

Fig. 9. EDS soil treated with Cu^{2+} and Pb^{2+}: typical gibbsite (containing 6% Cu^{2+} and 4% Pb^{2+}) and kaolinite.
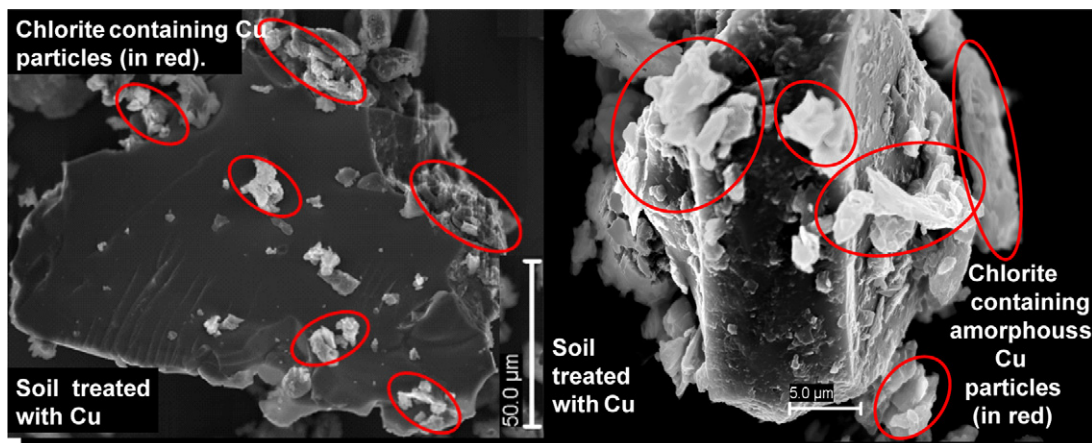
Fig. 10. Chlorite containing Cu^{2+} particles.

verifying the soil ion spatial distribution of heavy metals such as Pb^{2+} and Cu^{2+} are confirmed in this study.

3.2. Electron beam microscopy

The HR-TEM/EDS/SAED results combined with FE-SEM/EDS (Figs. 8–11) show that gibbsite plays a very important role in the fixation of both metals (Pb^{2+} and Cu^{2+}). These results are in agreement with those of previous studies [3].

It was found that both metals (Cu^{2+} and Pb^{2+}) are sorbed in the gibbsite, whose presence and abundance in the soil significantly increases the sorption capacity of both metals [3,17]. It was found that the gibbsite from contaminated soil samples contains 6% Cu^{2+} and 4% Pb^{2+}.

The samples that were only treated with Pb^{2+} clearly show the sorption of this ion in the gibbsite (Fig. 8), proving the previously found high correlation [18]. Similar results were observed in the chlorite (Fig. 10).

It is also important to note that the association of these metals with hematite has been proved (by HR-TEM/EDS) (Fig. 11). Several studies have shown that iron oxides significantly contribute to Cu^{2+} and Pb^{2+} sorption [38,39].

Moreover, the results obtained by FE-SEM and HR-TEM analysis revealed that when soil samples were contaminated with both Cu^{2+} and Pb^{2+} they have a higher affinity for Pb^{2+} sorption than for Cu^{2+} which is in agreement with the results of Harter and Naidu [40].
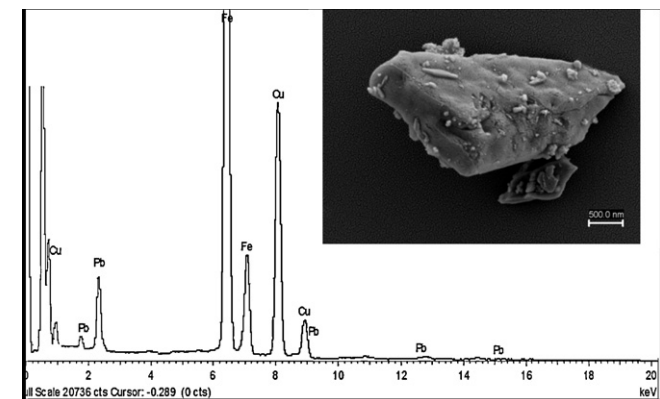
4. Conclusions

The soil has higher affinity for Pb^{2+} than for Cu^{2+}. The Pb^{2+} competes favorably for the sorption sites in these soils, mainly in the oxides and clay fraction. Cu^{2+} and Pb^{2+} were mainly associated with hematite, gibbsite, vermiculite and chlorite.

High-resolution microscopy studies combined with analysis by TOF-SIMS, batch experimental studies and statistical analysis are an effective tool to check the affinity of the soil components for cations, as well as competition between them for sorption sites.

This study will serve as a basis for further scientific research on the soil retention of heavy metals, as high-resolution microscopy makes it possible to check which soil components retain heavy metals (with high toxicity), thereby contributing to propose effective measures for the remediation of contaminated soil.

Acknowledgements

References

[1] D.L. Sparks, A.M. Scheidegger, D.G. Strawn, K.G. Scheckel, Kinetics and mechanisms of metal sorption at the mineral–water interface, in: D.L. Sparks, T.J. Grundl (Eds.), Mineral–Water Interfacial Reactions, ACS Symp., Series 715, Am. Chem. Soc., Washington, DC, 1999, pp. 108–135.

[2] R. Apak, Adsorption of heavy metal ions on soil surfaces and similar substances, in: A. Hubbard (Ed.), Encyclopedia of Surface and Colloid Science, Dekker, New York, 2002, pp. 385–417.

[3] F.A. Vega, E.F. Covelo, M.L. Andrade, A versatile parameter for comparing the capacities of soils for sorption and retention of heavy metals dumped individually or together: results for cadmium, copper and lead in twenty soil horizons, J. Colloid Interface Sci. 327 (2008) 275–286.

[4] F.X. Han, A. Banin, Long-term transformations and redistribution of potentially toxic heavy metals in arid-zone soils. II. Under the field capacity regime, Water Air Soil Pollut. 114 (1999) 221–250.

[5] F.X. Han, A. Banin, G.B. Triplett, Redistribution of heavy metals in arid-zone soils under a wetting–drying soil moisture regime, Soil Sci. 166 (2001) 18–28.

[6] E.F. Covelo, F.A. Vega, M.L. Andrade, Sorption and desorption of Cd, Cr, Cu, Ni, Pb and Zn by a Fibric Histosol and its organo-mineral fraction, J. Hazard. Mater. 159 (2008) 342–347.

[7] L.M. Dudley, J.E. McLean, T.H. Furst, J.J. Jurinak, Sorption of cadmium and copper from an acid mine waste extract by two calcareous soils: column studies, Soil Sci. 151 (1991) 121–135.

[8] P. Sipos, T. Németh, V. Kovács Kis, I. Mohai, Sorption of copper, zinc and lead on soil mineral phases, Chemosphere 73 (2008) 461–469.

Fig. 11. Hematite ultrafine particle containing Cu^{2+} and Pb^{2+} in soil treated with Pb^{2+} and Cu^{2+}.

[9] M. Komárek, J. Száková, M. Rohošková, H. Javorská, V. Chrastný, J. Balík, Copper contamination of vineyard soils from small wine producers: a case study from the Czech Republic, Geoderma 147 (2008) 16–22.

[10] M. Komárek, V. Ettler, V. Chrastný, M. Mihaljevič, Lead isotopes in environmental sciences: a review, Environ. Int. 34 (2008) 562–577.

[11] T. Németh, J. Jiménez-Millán, P. Sipos, I. Abad, R. Jiménez-Espinosa, Z. Szalaic, Effect of pedogenic clay minerals on the sorption of copper in a Luvisol B horizon, Geoderma 160 (2011) 509–516.

[12] N. Cavallaro, M.B. McBride, Zinc and copper sorption and fixation by an acid soil clay: effect of selective dissolutions, Soil Sci. Soc. Am. J. 48 (1984) 1050–1054.

[13] L.M. Shuman, Effect of organic matter on the distribution of manganese, copper, iron, and zinc in soil fractions, Soil Sci. 146 (1988) 192–198.

[14] P. Sipos, T. Németh, I. Mohai, I. Dódony, Effect of soil composition on sorption of lead as reflected by a study on a natural forest soil profile, Geoderma 124 (2005) 363–374.

[15] P. Sipos, T. Németh, V. Kovács Kis, I. Mohai, Association of individual soil mineral constituents and heavy metals as studied by sorption experiments and analytical electron microscopy analyses, J. Hazard. Mater. 168 (2009) 1512–1520.

[16] E.F. Covelo, F.A. Vega, M.L. Andrade, Simultaneous sorption and desorption of Cd, Cr, Ni, Cu, Pb and Zn in acid soils. I. Selectivity sequences, J. Hazard. Mater. 147 (3) (2007) 852–861.

[17] E.F. Covelo, F.A. Vega, M.L. Andrade, Simultaneous sorption and desorption of Cd, Cr, Ni, Cu, Pb and Zn in acid soils. II. Soil ranking and influence of soil characteristics, J. Hazard. Mater. 147 (3) (2007) 862–870.

[18] B. Cerqueira, E.F. Covelo, L. Andrade, F.A. Vega, The influence of soil properties on the individual and competitive sorption and desorption of Cu and Cd, Geoderma 162 (2011) 20–26.

[19] F.A. Vega, M.L. Andrade, E.F. Covelo, Influence of soil properties on the sorption and retention of cadmium, copper and lead, separately and together, by 20 soil horizons: comparison of linear regression and tree regression analyses, J. Hazard. Mater. 174 (2010) 522–533.

[20] R.F.K. Herzog, F. Viehboeck, Ion source for mass spectrography, Phys. Rev. 76 (1949) 855–856.

[21] A. Benninghoven, B. Hagenhoff, E. Niehuis, M.S. Surface, Probing real-world samples, Anal. Chem. 65 (1993) 630–640.

[22] A. Benninghoven, Chemical analysis of inorganic and organic surfaces and thin films by static time-of-flight secondary ion mass spectrometry (TOF-SIMS), Angew. Chem. Int. Ed. 33 (1994) 1023–1043.

[23] J. Grams, New Trends, Potentialities of TOF-SIMS in Surface Studies, Nova Science Publishers Inc., New York, 2007, p. 273.

[24] WRBSR, World reference base for soil resources, A framework for international classification correlation and communication, IUSS-ISRIC-FAO, World Soil Resources Reports 103, Rome, 2006, 146 pp.

[25] M.C. Rodríguez-Argüelles, R. Villalonga, C. Serra, R. Cao, M.A. Sanromán, M.A. Longo, A copper(II) thiosemicarbazone complex built on gold for the immobilization of lipase and laccase, J. Colloid Interface Sci. 348 (2010) 96–100.

[26] J. Ribeiro, D. Flores, C.R. Ward, L.F.S. Silva, Identification of nanominerals and nanoparticles in burning coal waste piles from Portugal, Sci. Total Environ. 408 (2010) 6032–6041.

[27] L.F.O. Silva, T. Moreno, X. Querol, An introductory TEM study of Fe-nanominerals within coal fly ash, Sci. Total Environ. 407 (2009) 4972–4974.

[28] S. Hayashi, T. Takahashi, K. Kanehashi, N. Kubota, K. Mizuno, S. Kashiwakura, T. Sakamoto, T. Nagasaka, Chemical state of boron in coal fly ash investigated by focused-ion-beam time-of-flight secondary ion mass spectrometry (FIB-TOF-SIMS) and satellite-transition magic angle spinning nuclear magnetic resonance (STMAS NMR), Chemosphere 80 (2010) 881–887.

[29] S.B. Abreu, W. Skinner, Predicting the surface chemistry contribution to the flotation recovery of chalcopyrite by TOF-SIMS, Miner. Eng. 24 (2011) 160–168.

[30] L.F.O. Silva, J.C. Hower, M. Izquierdo, X. Querol, Complex nanominerals and ultrafine particles assemblages in phosphogypsum of the fertilizer industry and implications on human exposure, Sci. Total Environ. 408 (2010) 5117–5122.

[31] L.F.O. Silva, C.R. Ward, J.C. Hower, M. Izquierdo, F. Waanders, M.L.O. Oliveira, Z. Li, R.S. Hatch, X. Querol, Mineralogy and leaching characteristics of coal ash from a major Brazilian power plant, Coal Combust. Gasification Prod. 2 (2010) 51–65.

[32] L.F.O. Silva, X. Querol, K.M. da Boit, S.F.O.D. Vallejuelo, J.M. Madariaga, Brazilian coal mining residues and sulphide oxidation by Fenton's reaction: an accelerated weathering procedure to evaluate possible environmental impact, J. Hazard. Mater. 186 (2011) 516–525.

[33] L.F.O. Silva, M. Wollenschlager, M.L.S. Oliveira, A preliminary study of coal mining drainage and environmental health in the Santa Catarina region, Brazil, Environ. Geochem. Health (N.Y.) 33 (2011) 55–65.

[34] L.F.O. Silva, M.L.S. Oliveira, E.R. Neace, J.M.K. O'Keefe, K.R. Henke, J.C. Hower, Nanominerals, ultrafine particles in sublimates from the Ruth Mullins coal fire, Perry County, Eastern Kentucky, USA, Int. J. Coal Geol. 85 (2011) 237–245.

[35] L.F.O. Silva, F. Macias, M.L.S. Oliveira, K.M. da Boit, F. Waanders, Coal cleaning residues and Fe-minerals implications, Environ. Monit. Assess. 172 (2011) 367–378.

[36] L.F.O. Silva, K. DaBoit, Nanominerals and nanoparticles in feed coal and bottom ash: implications for human health effects, Environ. Monit. Assess. 174 (2011) 187–197.

[37] ICDD, International Center for Diffraction Data, http://www.icdd.com (accessed 20.11.10).

[38] A. Kabata-Pendias, Trace Elements in Soils and Plants, CRC Press, Boca Raton, FL, USA, 2001.

[39] A.M. Moreno, J.R. Quintana, L. Pérez, J.G. Parra, Factors influencing lead sorption–desorption at variable added metal concentrations in Rhodoxeralfs, Chemosphere 64 (5) (2006) 758–763.

[40] R.D. Harter, R. Naidu, An assessment of environmental and solution parameter impact on trace-metal sorption by soils, Soil Sci. Soc. Am. J. 65 (2001) 597–612.